



**HAL**  
open science

## Soil carbon dioxide fluxes to atmosphere: the role of rainfall over CO<sub>2</sub> transport

Isabelle Delsarte, Grégory Cohen, Marian Momtbrun, Patrick Höhener, Olivier Atteia

### ► To cite this version:

Isabelle Delsarte, Grégory Cohen, Marian Momtbrun, Patrick Höhener, Olivier Atteia. Soil carbon dioxide fluxes to atmosphere: the role of rainfall over CO<sub>2</sub> transport. *Applied Geochemistry*, 2021, 127, pp.104854. 10.1016/j.apgeochem.2020.104854 . hal-03087039

**HAL Id: hal-03087039**

**<https://amu.hal.science/hal-03087039v1>**

Submitted on 5 Jan 2021

**HAL** is a multi-disciplinary open access archive for the deposit and dissemination of scientific research documents, whether they are published or not. The documents may come from teaching and research institutions in France or abroad, or from public or private research centers.

L'archive ouverte pluridisciplinaire **HAL**, est destinée au dépôt et à la diffusion de documents scientifiques de niveau recherche, publiés ou non, émanant des établissements d'enseignement et de recherche français ou étrangers, des laboratoires publics ou privés.

1 **Soil carbon dioxide fluxes to atmosphere: the role of rainfall to control CO<sub>2</sub> transport**

2 Isabelle DELSARTE<sup>1\*</sup>, Grégory COHEN<sup>1</sup>, Marian MOMTBRUN<sup>1</sup>, Patrick Höhener<sup>2</sup> and

3 Olivier ATTEIA<sup>1</sup>

4 <sup>1</sup> EA 4592 G&E, Bordeaux INP, 1 allée F. Daguin, 33607 Pessac, France

5 <sup>2</sup> Aix-Marseille Université - CNRS, Laboratoire Chimie Environnement UMR 7376, 3 place

6 Victor Hugo, 13331 Marseille, France

7 \*isabelle.delsarte@bordeaux-inp.fr

8 Abstract

9 In order to observe the relationships between the temporal variations of CO<sub>2</sub> surface  
10 fluxes and the CO<sub>2</sub> soil gas transport in soil profile before and during rainfall events, two  
11 experiments were conducted in a controlled natural environment at different time periods.  
12 These experiments consisted in injecting pure CO<sub>2</sub> in a lysimeter at 160 cm depth and  
13 simulating heavy rainfall event at its surface for 2 weeks. During the whole experiments, CO<sub>2</sub>  
14 soil gas concentrations and surface fluxes were continuously monitored. These measurements  
15 showed that the flux measured through the flux chamber were consistent with the concentration  
16 profiles. During simulated rainfall events, the concentrations and fluxes showed a clear change  
17 linked to the presence of water on the top of the water profile. The results clearly show a  
18 significant decrease of CO<sub>2</sub> flux to atmosphere induced by rainfall infiltration and consequential  
19 wash-out of the CO<sub>2</sub> present in the soil.

20 Keywords: CO<sub>2</sub> concentration, soil CO<sub>2</sub> flux, rainfall, soil gas concentration and fluxes  
21 monitoring

22

23 1. Introduction

24 The soil is the interface between the different environmental compartments (lithosphere,  
25 the atmosphere...), where fluxes of water, particles and gas are constantly exchanged. Due to  
26 past and current human activities, the composition of these fluxes was significantly altered, that  
27 imposes a threat to the environment and human health. During the last decades, special attention  
28 has been paid to gas exchanges at the soil-atmosphere interface. Indeed, the need to understand  
29 and monitor gas fluxes is ubiquitous in many areas of human activity. For example, on the  
30 carbon capture and storage sites, the monitoring of CO<sub>2</sub> fluxes is necessary to detect and  
31 quantify eventual leakages to the environment (Bernardo and Vries, 2011; Beaubien et al.,  
32 2013; Schroder et al., 2016; Elío et al., 2016). Following landfill gas emissions across the  
33 surface of landfills is also essential. Indeed, the landfill gas is ranked as the third highest source  
34 of global anthropogenic methane emissions (Yang et al., 2015) and contributes also to large  
35 CO<sub>2</sub> emissions. Another example concerns the contaminated sites, where measurement soil gas  
36 fluxes are often required as part of human health risk assessment of the site or when  
37 implementing a risk-based corrective approach (Hers et al., 2004).

38 Gas flux at the soil-atmosphere interface, can be directly measured using flux chambers  
39 methods (Bornemann, 1920; Klenbusch, 1986). These techniques are based on the  
40 measurement of the compound concentration increase inside an open-bottom chamber set up  
41 on the soil surface. The gas flux is then calculated by relating the concentration increase during  
42 a given time to the chamber volume and the concerned soil surface area. Due to the low cost of  
43 this non-intrusive method which is easy to set up, it has been widely used (Cotel et al., 2015;  
44 Elío et al., 2016; Jassal et al., 2005; Matthias et al., 1980; Norman et al., 1997; Reinhart et al.,  
45 1992; Rochette and Hutchinson, 2005; Viveiros et al., 2008). Indeed, this technique allows to  
46 carry out *in situ* measurements quickly and on a large number of points compared to other  
47 techniques (Schroder et al., 2016).

48           However, due to the soil heterogeneity resulting from the spatial and temporal  
49           variability of the physico-chemical soil properties such as moisture, the instantaneous fluxes  
50           measured in practice do not allow to easily determine the long term transport of vapours to the  
51           atmosphere (Bekele et al., 2014). Several authors observed seasonal variations of gas surface  
52           fluxes or soil gas concentrations (Elío et al., 2013; Kim et al., 2019). Indeed, these researchers  
53           observed the dependence of CO<sub>2</sub> fluxes with soil moisture variations which are likely to govern  
54           soil gas transport processes. Petersen et al. (1996) and Choi et al. (2005) observed that  
55           trichloroethene (TCE) gas-phase diffusive fluxes at soil surface were also sensitive to soil-water  
56           content modifications. Moisture content in the subsurface modifies the pore volume available  
57           for gas transport (Risk et al., 2002; Tillman and Smith, 2004; Palaia et al., 2018). Moisture  
58           content impacts the transport of gas phase in the soil by modifying soil tortuosity as well as the  
59           effective diffusivity and the dissolved quantity of the concerned compound in the aqueous phase  
60           (Conant et al., 1996; Hers et al., 2000; Jassal et al., 2005). In the literature, there is still an  
61           ongoing discussion about the different formulae used to link soil water content to the effective  
62           tortuosity (Hers et al., 2000; Werner et al., 2004). The heterogeneous distribution of soil  
63           moisture content has also a direct effect on subsurface gas concentration profile (Shen et al.,  
64           2013). Wetter soil layers could therefore have different effects such as reducing the gas  
65           diffusion from the source to the atmosphere or, conversely, increasing surface fluxes. It was  
66           also shown that rainfall duration, intensity, frequency and spatial variability has direct influence  
67           on gas fluxes (Fa et al., 2015; Lelli and Raco, 2017; Ma et al., 2012; Seo et al., 2020;  
68           Tommasone Pascale et al., 2015). In their study, Viveiros et al. (2008) showed that depending  
69           on the intensity of the rainfall, the soil CO<sub>2</sub> fluxes are different. Tommasone Pascale et al.  
70           (2015) observed the influence of rainfall events on soil radon (<sup>222</sup>Rn) concentration and  
71           concluded that time evolution of soil <sup>222</sup>Rn activities are markedly dependent on the rainfall  
72           history of the site.

73 While there is a general agreement on the importance of soil water content, there has  
74 been, to our knowledge, limited quantitative analysis related to its influence (Hers et al., 2000;  
75 Oh et al., 2019; Shen et al., 2013). Even if some field and / or numerical studies have considered  
76 some temporal effects on soil gas transport, a full explanation of the influence of rainfall events  
77 on soil gas concentrations and fluxes is still not available (Viveiros et al., 2008; Lewicki et al.,  
78 2009; Shen et al., 2012). However, understanding how these short and/or long-term variations  
79 modify soil gas transport processes is of major importance for precisely quantify long term gas  
80 fluxes at monitoring sites.

81 Therefore, the main objective of this study is to understand the relationships between  
82 the temporal variations of gas surface fluxes and the soil gas transport in soil profile before and  
83 during rainfall events. To this end, two experiments were conducted in a controlled natural  
84 environment. These experiments consisted in injecting pure CO<sub>2</sub> in a lysimeter and simulating  
85 rainfall event at its surface. During the whole experiments, CO<sub>2</sub> soil gas concentrations and  
86 surface fluxes were continuously monitored. The impact of natural rainfall events of different  
87 intensities and frequencies on CO<sub>2</sub> fluxes at the soil-atmosphere interface were also observed.

## 88 2. Materials and methods

### 89 2.1. Lysimeter description

90 The experiments were conducted in a lysimeter, a controlled natural environment  
91 (Figure 1). This lysimeter was set up in August 2014. Soil digging was conducted thanks to a  
92 mechanical shovel which removed and separated sequentially 50 cm depth soils layers until  
93 1.85 m depth. The retention tank ( $l \times w \times h = 1.35 \times 1.35 \times 0.8$  m) was then set-up. At the  
94 bottom of the tank, a grid was added allowing an easier water recovery. Moreover, a gooseneck  
95 system, connected to the bottom of the retention tank allows the control of the piezometric level  
96 and the quantification of outflowing water. After the set-up of the retention tank, the soil was  
97 manually put back in place backward in order to respect as much as possible the original soil

98 configuration. Each soil layer of 10 cm height was compacted. In the centre of lysimeter, six  
 99 gas probes were set up during this backfill, placing them at specific depths (0.4, 0.8, 1.0, 1.2,  
 100 1.4 and 1.6 m depth) (Figure 1). To avoid vertical preferential paths, their tubes were placed in  
 101 the ground horizontally until the manhole. Thus, the soil removed during the lysimeter  
 102 installation was returned to respect as much as possible its initial structure. The soil matrix is  
 103 an alluvial sand from the Aquitaine basin (France). Moreover, the soil does not contain calcite  
 104 (<1%) over the entire vertical profile of the lysimeter and the CEC capacity varies from 15  
 105 mmol<sub>c</sub>/kg at 20 cm to 1-2 at 1 m depth.

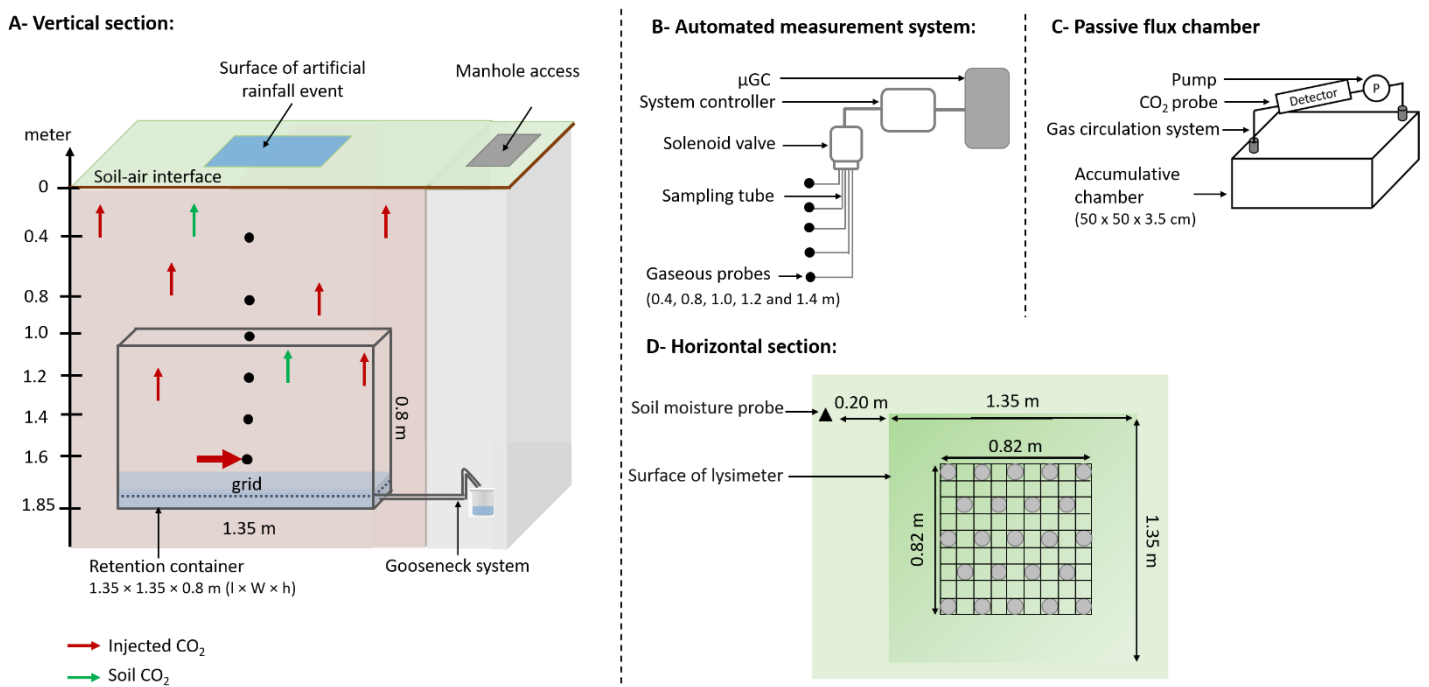


Figure 1. General description of the lysimeter. A- Vertical section of the lysimeter: a grid rested on the bottom of the tank and allowed the porous medium to be separated from the water. The black dots represent the location of the gas probes. B- Automated measurement system for continuous monitoring of CO<sub>2</sub> concentrations in the soil. C- Schematic of passive flux chamber used to determine surfaces fluxes. D- Horizontal section of the lysimeter: the blue and grey dots represents the location of the piezometer and the tubes used for artificial the rainfall event, respectively.

## 107 2.2. Hydrological properties of porous media

### 108 2.2.1. Determination of soil porosity and water content by soil coring

109 The initial water content, the residual water saturation and the porosity of the porous  
110 medium were experimentally determined. Soil cores were taken from the experimental plot next  
111 to the lysimeter at 0.2, 0.5 and 1.0 m depth. The sampling tool consists in a sampling tube on  
112 which is added a corer (S x L: 11.95 x 14.8 cm<sup>2</sup>). A pilot hole is previously made with a manual  
113 auger to the desired depth. The tube is then driven into the ground either directly or with a  
114 sledgehammer. Soil cores were first slowly saturated with tap water for 24 h before being placed  
115 in the oven at 105°C for 24 h (Wilke, 2005). At every step, soil cores were weighted.

### 116 2.2.2. Transient water content measurement

117 Soil moisture content was determined by using moisture probes (120 cm; Drill & Drop  
118 Probe, SDI-12, Sentek) composed by ten moisture sensors. Thus, soil moisture was measured  
119 every 10 cm from 7 to 97 cm depth. To avoid preferential gas flow and damage of gas sample  
120 probes, this probe was set up 20 cm next to the lysimeter (Figure 1). The soil matrix at this  
121 emplacement is the same as the one inside the lysimeter. The soil moisture probes were  
122 calibrated *in situ* by an analysis of their temporal signal variations with respect to the cumulative  
123 amount of water infiltrated during the artificial rainfall event.

## 124 2.3. CO<sub>2</sub> soil gas concentration measurements

125 CO<sub>2</sub> soil gas concentrations were continuously monitored with the use of a custom  
126 automated system. This automated system is composed of a micro-GC (CP-4900, Varian Inc.),  
127 a system controller (M3 Essential extensibles, Crouzet) and a solenoid valve (EMHMA-CE,  
128 Vici Valco) directly connected to the five soil gas probes (0.4, 0.8, 1.0, 1.2 and 1.4 m depth)  
129 (Figure 1). The micro-GC is equipped with a PPQ column to separate CO<sub>2</sub>. The general relative  
130 uncertainty for the quantification of CO<sub>2</sub> with this method is less than 5%. Tubes of 2.50 m

131 with an inner diameter of 0.5 mm were used to connect each gas probe to the automated system.  
132 For each analysis, a gas sample of 70 mL was collected from the soil by micro-GC pumping  
133 system. The dead volumes of the gas tubes were taken under consideration to determine the  
134 optimal sampling volume.

#### 135 2.4. Gas flux monitoring at the soil surface using a flux chamber

136 A Passive Flux Chamber (PFC) (50 x 50 x 3.5 cm (L x W x H)) was used to monitor  
137 CO<sub>2</sub> gas fluxes at the centre of the lysimeter surface (Figure 1). A sealed pumping system with  
138 a flowrate of about 500 mL min<sup>-1</sup> allows gas circulation from the accumulation chamber to the  
139 detector and its homogenization inside the PFC. The CO<sub>2</sub> concentrations were measured with  
140 a CO<sub>2</sub> probe (GMT222 Vaisala) placed in the PFC gas circulation system. To correct the CO<sub>2</sub>  
141 probe values, an intercomparison with the micro-GC was realized. This step was realized on  
142 several CO<sub>2</sub> concentrations (Information is available in the Supplementary information).

143 The soil surface CO<sub>2</sub> gas fluxes ( $F_{CO_2}$  in g m<sup>-2</sup> min<sup>-1</sup>) were calculated during the transient  
144 state of gas transfer in the flux chamber headspace as follows (Matthias et al. 1980):

$$145 F_{CO_2} = \frac{V_{ch}}{A_{ch}} \times \frac{dC}{dt} \quad (1)$$

146 Where  $dC$  (g m<sup>-3</sup>) is the variation of the CO<sub>2</sub> vapour concentration in the chamber during  
147  $dt$  (min),  $V_{ch}$  (m<sup>3</sup>) is the net volume of the chamber, and  $A_{ch}$  (m<sup>2</sup>) the covered soil surface area.

148 Based on the principle of gas accumulation within the chamber, the initial slope of the  
149 measured gas concentration-time curve is generally used to quantify the time derivative of Eq.  
150 (1) (Cotel et al. 2015).

151 Uncertainties in the experimental CO<sub>2</sub> mass fluxes measured with this flux chamber  
152 were calculated according to the method used by Cotel et al. (2015). Thus, uncertainties in the  
153 flux measurements were determined using a total derivative expansion for correlated variables  
154 of  $F_{CO_2}$ :



155 
$$\frac{\Delta F_{CO_2}}{F_{CO_2}} = \sqrt{\left(\frac{\Delta(dC/dt)}{dC/dt}\right)^2 + \left(\frac{\Delta V_{ch}}{V_{ch}}\right)^2 + \left(\frac{\Delta A_{ch}}{A_{ch}}\right)^2} \quad (2)$$

156 Considering uncertainties of 5%, 4% and 8% for CO<sub>2</sub> detector measurements, PFC section and  
 157 volume, respectively, the total uncertainty in the measured fluxes is about 10.25%.

158 **2.5.Experimental conditions**

159 The same experiment was realized at two different times of the year, in February and  
 160 October 2019. The timeline of both experiments is presented in Figure 2. For each experiment,  
 161 the CO<sub>2</sub> injection began at day 0. When the CO<sub>2</sub> concentration gradient was stabilized, an  
 162 artificial rainfall event was realized at 8.6 d for the 1<sup>st</sup> experiment and at 6 d for the second (cf.  
 163 2.5.2). For the 2<sup>nd</sup> experiment, a natural rainfall event followed the artificial one at 9 d. During  
 164 the experiments, the atmospheric pressure varied between 1018 and 1031 hPa for the 1<sup>st</sup>  
 165 experiment and between 992 and 1023 hPa for the 2<sup>nd</sup> experiment.

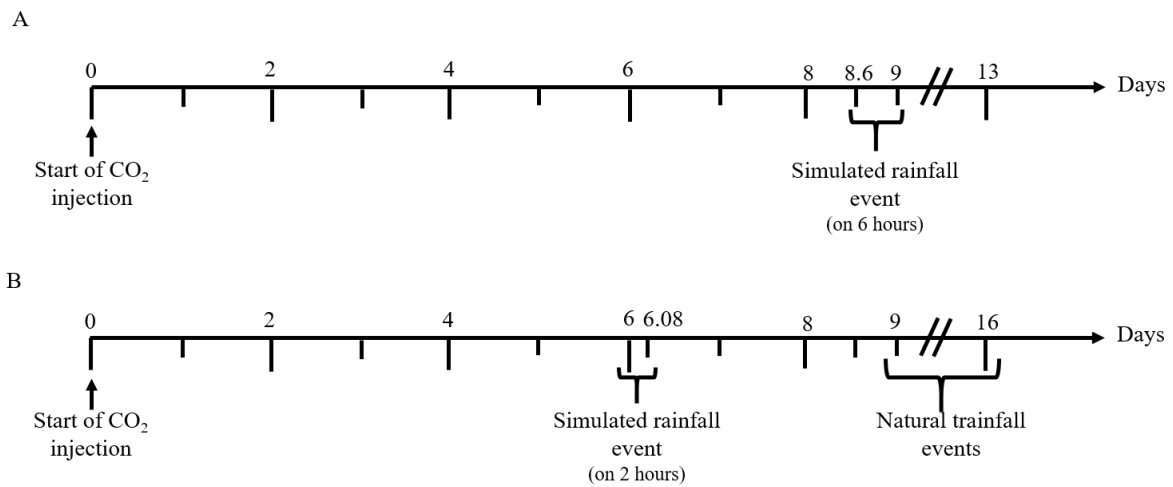


Figure 2. Timelines of the experiment realized in February 2019 (A) and in October 2019 (B).

166

167 **2.5.1. Gas injection conditions**

168 The gas injection was conducted with a bottle of CO<sub>2</sub> (99.7% Air Liquide) equipped  
 169 with a flow controller set at about 0.3 L.min<sup>-1</sup>. The gas was injected inside the retention tank at  
 170 160 cm depth of the lysimeter for 2 weeks.

171 2.5.2. Artificial rainfall event

172 For the two experiments, an intense rainfall event of about 100 mm of tap water was  
173 simulated during respectively 6 h and 2 h. The rainfall event was conducted in the centre of the  
174 lysimeter over a surface of  $0.82 \times 0.82$  m ( $0.67$  m<sup>2</sup>) leading to a total of 69 L. On this surface,  
175 23 tubes (inner diameter: 8 cm; H: 15 cm) were placed regularly on a regular mesh (Figure 1)  
176 and pressed 2 cm deep. These tubes allowed the homogeneous injection of tap water in soil (12  
177 x 250 mL / tube). The water was recovered at the outlet of the lysimeter through the gooseneck  
178 system (Figure 1). During the 2<sup>nd</sup> experiment, the same amount of water was injected in the  
179 centre of the lysimeter and an equivalent artificial rainfall event was also realized around the  
180 moisture probe. The rainfall event around the latter was conducted over a surface of  $0.63 \times$   
181  $0.63$  m leading to a total of 42 L. Given the proximity of the probe to the lysimeter,  
182 approximately 50% of the quantity of water injected could be collected at the outlet of the  
183 lysimeter, *i.e.* the equivalent of 90 L.

184 2.6. Calculation of the CO<sub>2</sub> mass balance

185 The domain considered for determining the approximate mass balance is the surface  
186 covered by the artificial rainfall event ( $0.672$  m<sup>2</sup>) across a depth of 80 cm, equivalent to a  
187 volume of 538 L. This domain is divided over depth in 16 equal subdomains ( $l \times w \times h = 82 \times$   
188  $82 \times 5$  cm). Each subdomain was characterised by the porosity, soil moisture content, gas phase  
189 volume as well as CO<sub>2</sub> soil concentrations in aqueous and gaseous phase.

190 According to porosities determined by soil coring method, a porosity of 0.33 was  
191 considered for the subdomains located between 0 to 0.5 m depth and 0.29 for the others located  
192 between 0.5 to 0.8 m depth. Soil moisture content of each subdomains was estimated based on  
193 soil moisture profile data allowing to calculated water phase volume ( $V_{aqueous\ phase}$ ):

194 
$$V_{aqueous\ phase} = \theta_{water} \times V_{subdomain} \quad (3)$$

195 Where  $\theta_{water}$  (-) is the volumetric soil water content and  $V_{subdomain}$  (L) is the volume of the  
196 subdomain.

197 The gas phase volume was then calculated as follows:

$$198 \quad V_{gaseous\ phase} = (\theta - \theta_{water}) \times V_{subdomain} \quad (4)$$

199 Where  $\theta$  (-) is the total connected porosity.

200  $CO_2$  mass in the gaseous phase in each subdomain was determined based on  $CO_2$  profiles  
201 data (Figure 5) and linear interpolation method. Assuming that in the soil the equilibrium  
202 between aqueous and gaseous phase was instantaneous, Henry's law was used to calculate the  
203  $CO_2$  mass in the aqueous phase ( $m_{aqueous\ phase}$ ):

$$204 \quad m_{aqueous\ phase} = (C_{gaseous\ phase} \times H^{cc}) \times V_{aqueous\ phase} \quad (5)$$

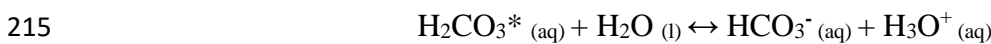
205 Where,  $H^{cc}$  is the dimensionless Henry solubility ( $C_a/C_g$ ). According to Sander et al. (2011) the  
206  $H^{cc}$  value is 0.818 at 25°C.

207 However, the  $H^{cc}$  value can change according to the buffering capacity (or alkalinity) of  
208 soil water which is the water capacity for solutes it contains to react with and neutralize acid.  
209 Thus, in contact with water,  $H_2O$  (l) and  $CO_2$  (g) form a carbonic acid molecule  $H_2CO_3$  (aq)  
210 according to the carbonation reaction:

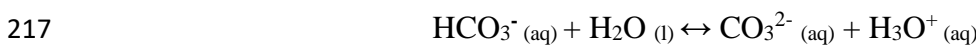


212 Where  $H_2CO_3^*$  represents the total concentration of dissolved  $CO_2$  and  $H_2CO_3$ .

213 As  $H_2CO_3$  (aq) is an acid, it reacts to form a bicarbonate ion  $HCO_3^-$  (aq) and a solvated  
214 proton  $H_3O^+$  (aq):



216 Then:



218 The previous reactions increase the apparent solubility of CO<sub>2</sub>. These dissolutions can  
 219 also be increased in presence of calcite. However, the Bernard calcimeter method showed that  
 220 the level of calcite in the soil studied was inferior to the quantification level (0.1%) (Rodier,  
 221 1976). Thus, from the alkalinity, pH and CO<sub>2</sub> added in the media, an apparent Henry constant  
 222 ( $H_{app}^{cc}$ ) can be calculated. Before and during the CO<sub>2</sub> injection (at steady state), alkalinity  
 223 measurements were realized by titration method (Table 1) on the water recovered at the outlet  
 224 of the lysimeter (Rodier, 1976). Alkalinity at 0.4 m and 0.8 m was estimated based on CO<sub>2</sub>  
 225 concentration profile at steady state (Figure 5) and alkalinity in the outflowing water using a  
 226 linear interpolation (Table 1). According to this method, the average value of  $H_{app}^{cc}$  estimated is  
 227 1.151 at 15°C.

228 Table 1. Parameters of the water recovered at the outlet of the lysimeter before and during the  
 229 CO<sub>2</sub> injection at steady state.

Experiment		at 0 d	At steady state		
Depth (m)		1.85	1.85	0.8	0.4
Soil	CO <sub>2</sub> gas concentration (% Vol CO <sub>2</sub> )	0.30	99.70	20.73	4.55
	CO <sub>2</sub> gas concentration added <sup>a</sup>	/	99.40	20.43	4.25
Aqueous phase	pH	7.39	6.41		
	Alkalinity (mol L <sup>-1</sup> )	0.0034	0.0256	/	/
	H <sub>2</sub> CO <sub>3</sub> concentration (mol L <sup>-1</sup> ) <sup>a</sup>	0.0004	0.0259	/	/
	HCO <sub>3</sub> <sup>-</sup> concentration added (mol L <sup>-1</sup> ) <sup>b</sup>	/	0.0222 <sup>a</sup>	0.0046	0.0009
	H <sub>2</sub> CO <sub>3</sub> concentration added (mol L <sup>-1</sup> ) <sup>c</sup>	/	0.0255 <sup>b</sup>	0.0052	0.0011

230 <sup>a</sup>  $10^{-(pKa \times \log([HCO_3^-]) - pH)}$  with pKa = 6.415 at 15°C

231 <sup>b</sup>  $[HCO_3^-]_{added} = ([HCO_3^-]_{at\ steady\ state} - [HCO_3^-]_{at\ 0\ d}) \times \% \text{ CO}_2 \text{ gas concentration added}$

232 <sup>c</sup>  $[H_2CO_3^*]_{added} = ([H_2CO_3^*]_{at\ steady\ state} - [H_2CO_3^*]_{at\ 0\ d}) \times \% \text{ CO}_2 \text{ gas concentration added}$

233

234 3. Results

235 3.1. Artificial rainfall event monitoring

236 Figure 3 shows the evolution of soil moisture content as a function of depth at different  
237 periods: before and during the artificial rainfall event. For the 2<sup>nd</sup> experiment, the initial soil  
238 moisture content was different than for the 1<sup>st</sup> experiment (Figure 3).

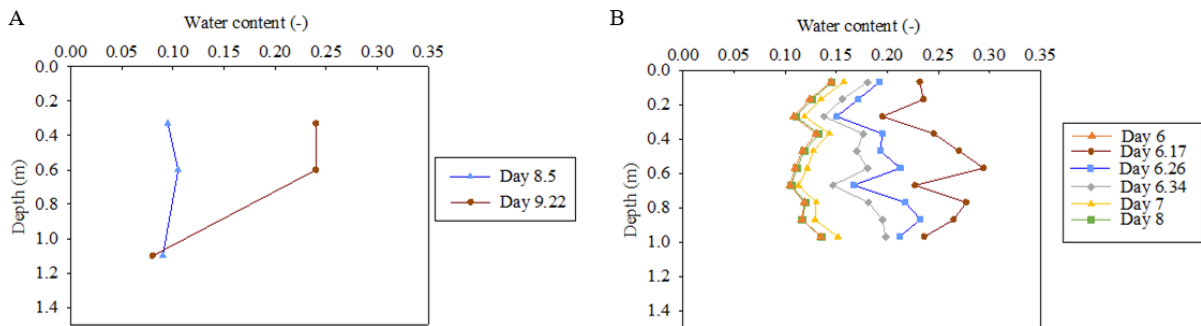


Figure 3. Spatial variation along vertical profile for soil moisture during and after the artificial rainfall event in February 2019 (A) and October 2019 (B) experiments.

239

240 Indeed, initial moisture content was in average of 0.097 for the February experiment  
241 and 0.12 for the 2<sup>nd</sup> experiment. Even if, water content varies in function of the depth, a  
242 consistent evolution of the profiles was observed during and after the rainfall event.

243 Figure 4 presents the cumulative outflow of water recovered at the outlet of the  
244 lysimeter. Two days after the artificial rainfall event, only 50% of the water amount injected  
245 was collected for the 1<sup>st</sup> experiment while this value was 92% for the 2<sup>nd</sup> experiment for the  
246 same duration. This difference may be linked to initial soil moisture content which was higher  
247 during the 2<sup>nd</sup> experiment (Figure 3).

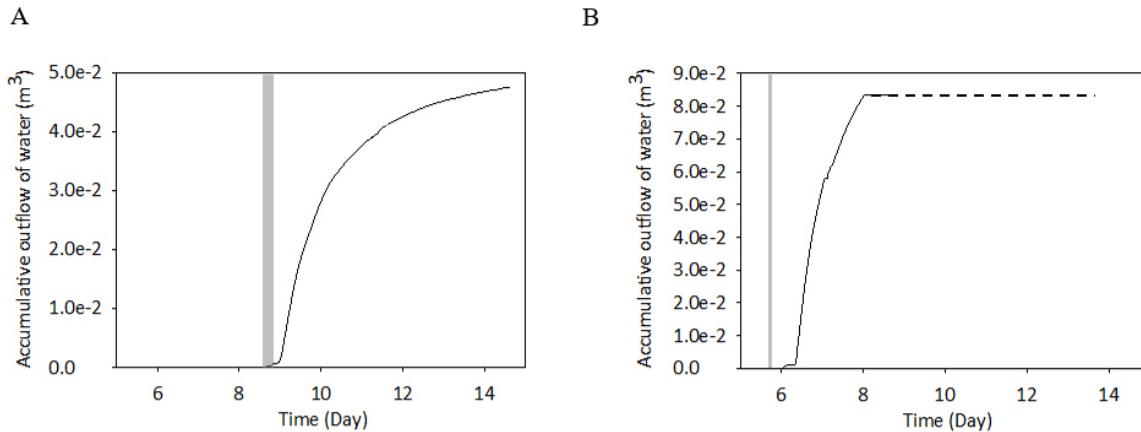


Figure 4. Cumulative outflow obtained during and after the artificial rainfall event in February 2019 (A) and October 2019 (B). The artificial rainfall events are highlighted with a grey area. The dotted lines indicate a data acquisition problem.

248

### 249 3.2. Soil CO<sub>2</sub> concentrations

250 Figure 5 presents the evolution of CO<sub>2</sub> soil gas concentrations as a function of depth at  
 251 different periods during the gas injection, until CO<sub>2</sub> profile stabilization. Measures were  
 252 realized before the CO<sub>2</sub> injection for baseline data. The CO<sub>2</sub> profiles obtained were like that  
 253 presented on Figure 5 at day 0 with a low CO<sub>2</sub> content  $\approx 0.3$  vol %. During the injection, CO<sub>2</sub>  
 254 content between 0.4 and 1.4 m depth respectively increased until 5 and de making the CO<sub>2</sub>  
 255 produced by the soil respiration negligible.

256 The CO<sub>2</sub> concentration at 0 m depth corresponds to the atmospheric concentration of  
 257 CO<sub>2</sub>. For the first experiment, the CO<sub>2</sub> stabilization in the soil occurred about 4 days after the  
 258 injection began (Figure 5-A). For the second experiment, the stabilization occurred later, about  
 259 5-6 days after the injection started. Indeed, even if the overall profile seems to be stable at day  
 260 4, CO<sub>2</sub> concentration at 0.4 m depth still varied after day 4 in the 2<sup>nd</sup> injection (Figure 5-B).  
 261 Moreover, during the injection, a change of slope at 0.8 m depth was observed. Due to its  
 262 density, CO<sub>2</sub> gas (1.83 instead of 1.21 kg m<sup>-3</sup> for air), may have accumulated in the lysimeter,  
 263 *i.e.* between 1.05 and 1.85 m depth, and the concentrations at 0.8 m may be influenced by dense  
 264 CO<sub>2</sub> flowing laterally from the lysimeter to the surrounding soil. This may explain the change

265 of CO<sub>2</sub> concentration slope observed at 0.8 and 0.4 m. Indeed, compared to diffusion, the  
 266 density effect can be neglected only for very low concentrations. Thus, the interpretation of  
 267 obtained results focused above all on the first 0.8 m of the lysimeter.

268

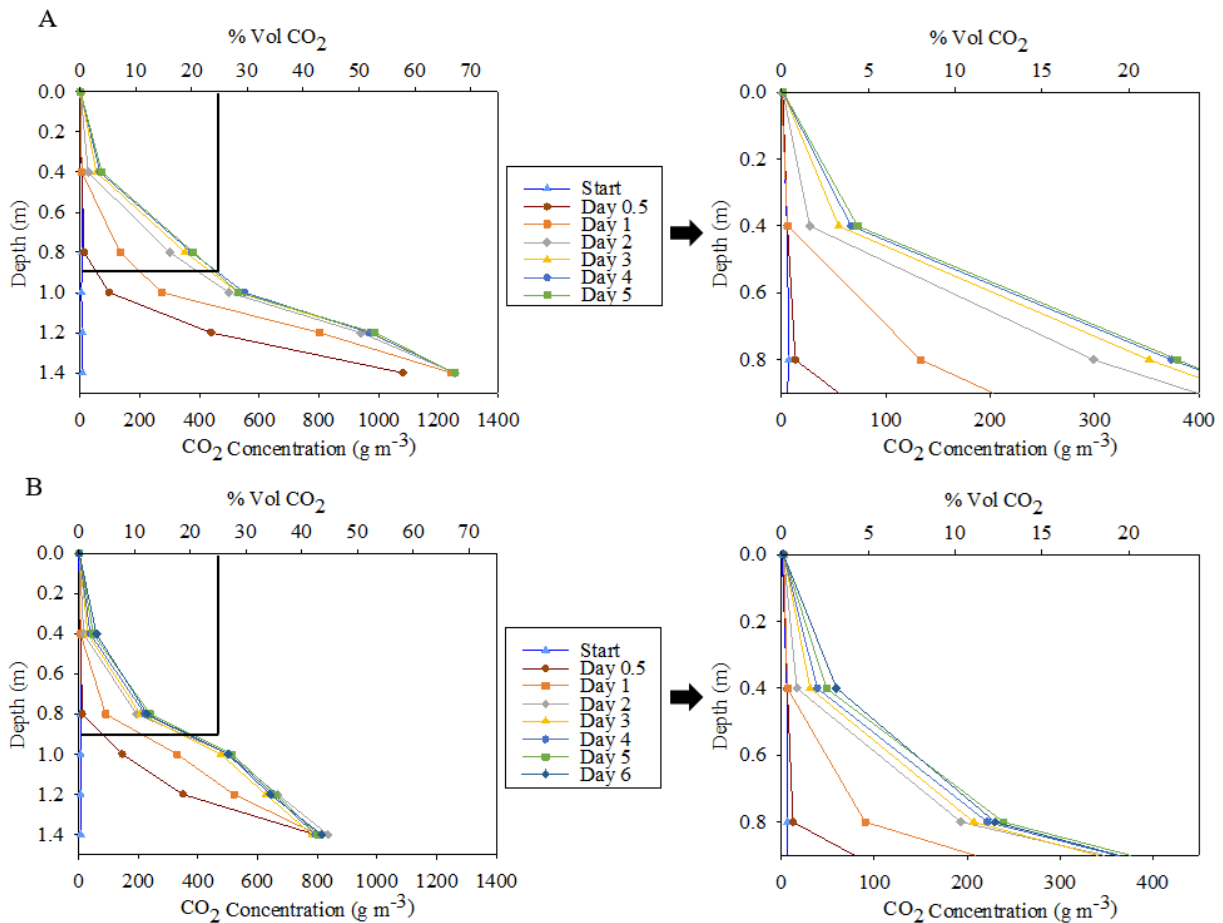


Figure 5. Evolution of CO<sub>2</sub> concentration profile at different period during the CO<sub>2</sub> injection in February 2019 (A) and in October 2019 (B). For A and B, the figure on the right is the inset of the figure on the left.

269 The temporal evolution of CO<sub>2</sub> soil gas concentrations is presented in Figure 6. In the  
 270 left part of each graph, the increase of CO<sub>2</sub> soil concentrations is clearly observed during the  
 271 beginning of the injection. The CO<sub>2</sub> gas concentrations at 0.4 and 0.8 m depth respectively  
 272 increased to 80 and 380 g m<sup>-3</sup> for the February experiment and to 50 and 230 g m<sup>-3</sup> for the 2<sup>nd</sup>  
 273 experiment. The grey part of graphs related to rainfall events will be described below.

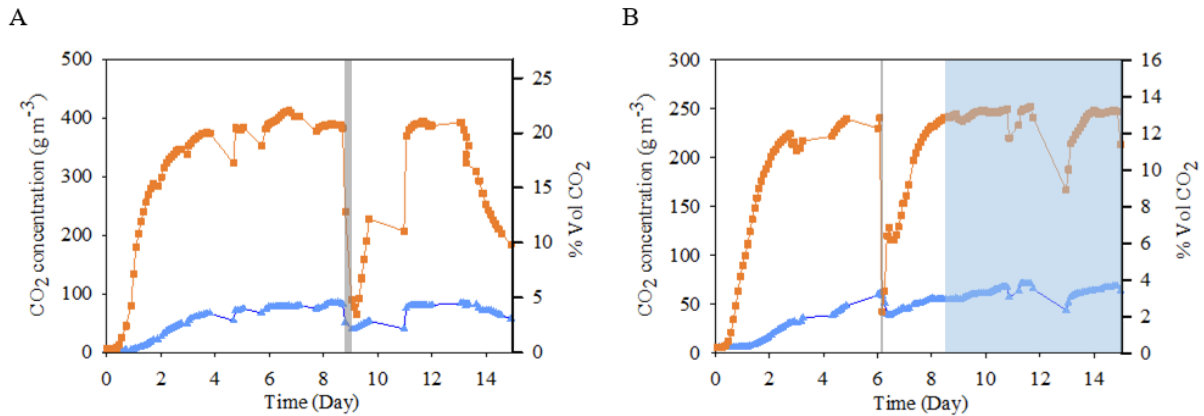


Figure 6. Times series for CO<sub>2</sub> soil gas concentrations measured at 0.4 (blue dots) and 0.8 m (orange dots) depth, in the centre of the lysimeter during the CO<sub>2</sub> injection in February 2019 (A) and in October 2019 (B). The artificial and natural rainfall events are underlined by a grey and blue area, respectively.

274

275           After the artificial rainfall event, the CO<sub>2</sub> profiles showed a significant modification  
 276 linked to the presence of water at the top of the lysimeter. In fact, a clear decrease of CO<sub>2</sub> gas  
 277 concentrations was observed, especially at 0.8 m depth (Figure 6 and 7). During the 1<sup>st</sup>  
 278 experiment, the CO<sub>2</sub> concentration at this depth decreased rapidly from 388 to 65 g m<sup>-3</sup>. This  
 279 minimum CO<sub>2</sub> concentration was measured 14 h after the beginning of the rainfall event and  
 280 represents a 5.9-fold decrease (Figure 7). Then, CO<sub>2</sub> concentrations increased and reached their  
 281 previous concentrations after two days. For the 2<sup>nd</sup> experiment, the CO<sub>2</sub> minimum concentration  
 282 was reached faster than for the 1<sup>st</sup> experiment. Indeed, the CO<sub>2</sub> concentration at this depth  
 283 decreased rapidly from 240 to 42 g m<sup>-3</sup>. This minimum CO<sub>2</sub> concentration was measured 4 h  
 284 after the beginning of the rainfall event and represents a 5.6-fold decrease. Then, the CO<sub>2</sub>  
 285 profiles returned to the steady state after 2.75 and 2 days for 1<sup>st</sup> and 2<sup>nd</sup> experiment, respectively  
 286 (Figure 7).

287           The CO<sub>2</sub> gas concentrations variations can be analysed in relation with soil moisture  
 288 content change for the second rainfall event (Figure 3). The highest soil moisture contents were  
 289 observed at 6.17 d when the CO<sub>2</sub> gas concentration at 0.8 m depth was the lowest. Moreover,



290 the moisture content profile turned back to steady state after 2 days as for CO<sub>2</sub> concentration  
 291 profile (Figure 3 and 7).

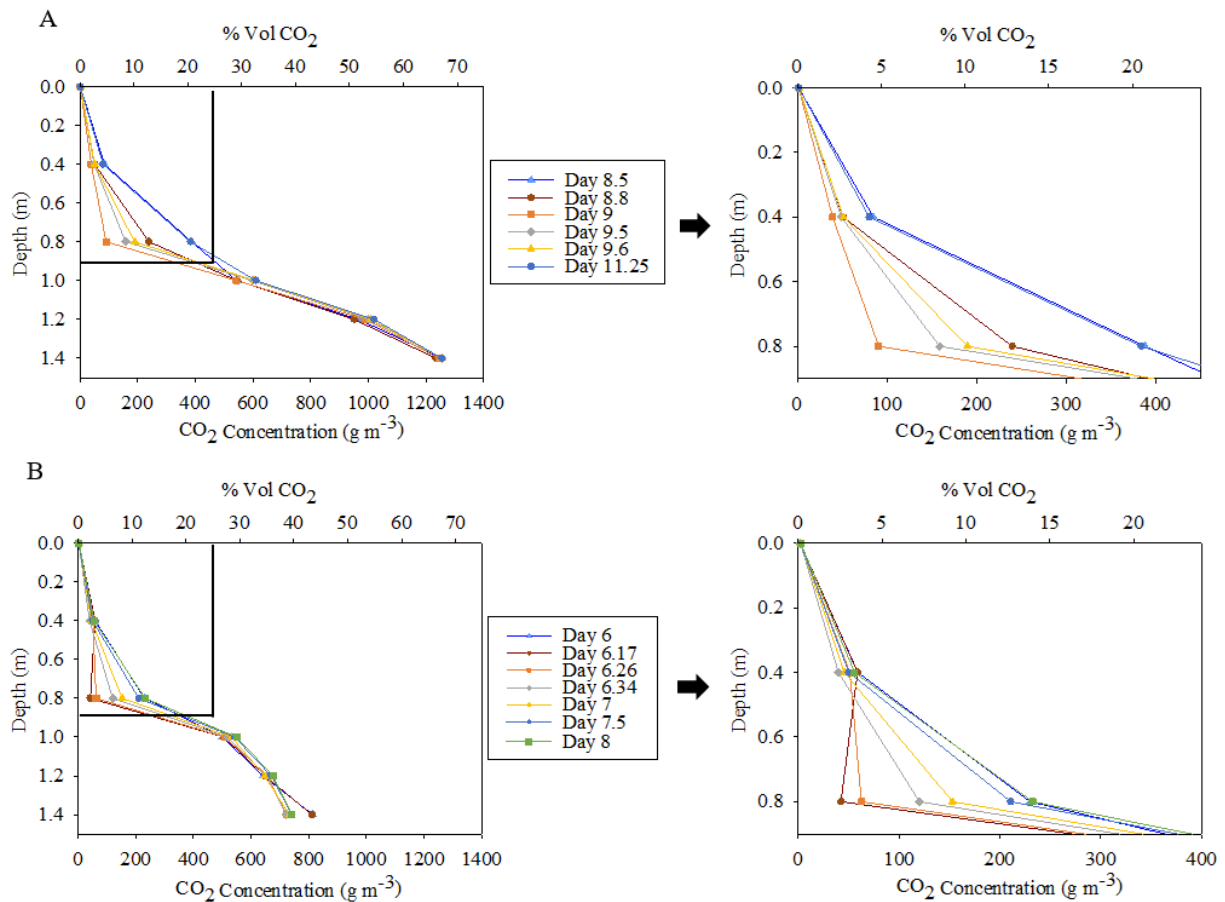


Figure 7. Evolution of CO<sub>2</sub> concentration profile at different period after the rainfall event, at 9 d for February 2019 (A) and at 6.08 d for October 2019 (B). For A and B, the figure on the right is the inset of the figure on the left.

292

### 293 3.3. CO<sub>2</sub> soil surface fluxes

294 The temporal evolution of CO<sub>2</sub> fluxes at lysimeter surface are presented in Figure 8. For  
 295 the 1<sup>st</sup> experiment, the measured CO<sub>2</sub> fluxes increased until a stabilization around 35 mg m<sup>-2</sup>  
 296 min<sup>-1</sup> which occurred about 5 days after injection began. For the 2<sup>nd</sup> experiment, the measured  
 297 CO<sub>2</sub> fluxes increase until about 40 mg m<sup>-2</sup> min<sup>-1</sup>. The fluxes measured across the surface were  
 298 greatly inferior compared to the injected CO<sub>2</sub> flux because part of injected CO<sub>2</sub> escapes laterally  
 299 and another part accumulates at depth.

300 After the artificial rainfall events, a significant decrease of CO<sub>2</sub> fluxes was noticed for  
 301 both experiments. They dropped from 35 to below 10, and from 40 to 1 mg m<sup>-2</sup> min<sup>-1</sup> for 1<sup>st</sup> and  
 302 2<sup>nd</sup> experiment (Figure 8), respectively. After these events, the CO<sub>2</sub> fluxes previously obtained  
 303 at steady state were not reached again, while the soil CO<sub>2</sub> concentrations reached back their  
 304 original values (Figure 7).

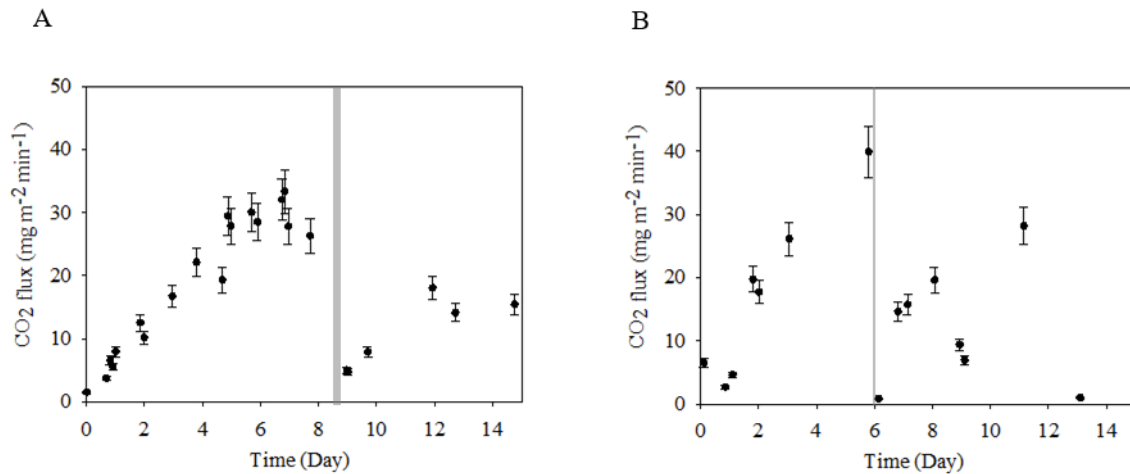


Figure 8. Times series of CO<sub>2</sub> soil surface fluxes, in the center of the lysimeter during the CO<sub>2</sub> injection in February 2019 (A) and in October 2019 (B). The artificial rainfall events are highlighted with a grey area.

305

### 306 3.4. CO<sub>2</sub> mass balance

307 To understand the influence of rainfall events on surface CO<sub>2</sub> gas fluxes, an approximate  
 308 mass balance was calculated for both experiments. This mass balance is based on CO<sub>2</sub> profiles  
 309 data obtained at the steady state (at 8.5 d and 6 d for event 1 and 2, respectively) and after the  
 310 artificial rainfall events (at 9.22 d for event 1 and at 6.17 and 6.34 d for event 2) (Table 2),  
 311 considering the surface covered by the artificial rainfall event (0.67 m<sup>2</sup>) across a depth of 80 cm.  
 312 CO<sub>2</sub> mass in the aqueous phase was calculated with a standard H<sup>cc</sup> value (Sander et al., 2011)  
 313 and  $H_{app}^{cc}$  determined according to the alkalinity data.

314

315

316 Table 2. Estimated mass balance between the end of steady state of CO<sub>2</sub> profile and the end of  
 317 the artificial rainfall event.

		Zone characteristics				
Area considered (m <sup>2</sup> )		0.672				
Investigated volume (0 to 0.8 m depth) (L)		538				
Pore volume <sup>a</sup> (0 to 0.8 m depth) (L)		170.18				
Media	Experiment	1st		2nd		
		At steady state at 8.5 d	After artificial rainfall event at 9.22 d	At steady state at 6 d	After artificial rainfall event at 6.17 d    at 6.34 d	
Soil	Volume of soil gaseous phase (L)	118.31	46.46	105.59	33.65	89.57
	Volume of the soil aqueous phase (L)	51.87	123.72	64.59	136.53	80.61
	CO <sub>2</sub> mass in the gaseous phase (g)	16.55	1.82	9.99	1.3	4.16
	CO <sub>2</sub> mass in the aqueous phase with H <sup>cc</sup> = 0.818 (g)	6.70	3.92	4.97	4.96	4.17
	CO <sub>2</sub> mass in the aqueous phase with H <sup>cc</sup> = 1.151 (g)	9.43	5.52	6.99	6.98	5.86
Interface soil/air	CO <sub>2</sub> Flux (mg m <sup>-2</sup> min <sup>-1</sup> )	29.4 ± 3.8	5.69 ± 0.74	39.9 ± 5.19	0.79 ± 0.1	4.8 ± 0.62
	CO <sub>2</sub> flow (g min <sup>-1</sup> )	0.020	0.004	0.027	0.0005	0.003
Mass Balance c		1st		2nd		
		9.22 d - 8.5 d		6.17 d - 6 d	6.34 d - 6.17 d	
Soil	Δ CO <sub>2</sub> mass in the gaseous phase (g)	-14.73		-8.69	2.86	
	Δ CO <sub>2</sub> mass in the aqueous phase with H <sup>cc</sup> = 0.818 (g)	-2.78		-0.01	-0.79	
	Δ CO <sub>2</sub> mass in the aqueous phase with H <sup>cc</sup> = 1.151 (g)	-3.91		-0.01	-1.12	
Interface soil/air	Δ CO <sub>2</sub> mass (g)	16.59 ± 2.16		6.48 ± 0.84	0.66 ± 0.9	

318 <sup>a</sup> Determined according to CO<sub>2</sub> concentration profile at steady state

319 <sup>b</sup> Determined according to CO<sub>2</sub> concentration profile after the artificial rainfall event

320

321            During the 1<sup>st</sup> experiment, at steady state (8.5 d), the considered soil volume contained  
 322 between 23.25 and 29.95 g of CO<sub>2</sub> with 16.55 g gaseous phase and between 6.70 and 13.40 g  
 323 in aqueous phase. After the artificial rainfall event, at 9.22 d, the total CO<sub>2</sub> mass contained in  
 324 considered soil volume decreased drastically. Indeed, the soil only contained between 5.74 and  
 325 9.61 g (about 3.6 times less than at steady state) with 1.82 g gaseous phase and between  
 326 3.92 and 7.79 g in aqueous phase. According to this mass balance, the mass of CO<sub>2</sub> lost in the  
 327 gas phase between 8.5 and 9.22 d would have been moved to the atmosphere at the top of the  
 328 investigated volume. In fact, according to CO<sub>2</sub> flux measurements, the CO<sub>2</sub> amount emitted at  
 329 the soil/air interface during this period was 16.59 ± 2.16 g, corresponding rather well to the  
 330 mass of CO<sub>2</sub> lost in the gas phase of about 14.73 g (Table 2). Concerning, the CO<sub>2</sub> amount in  
 331 aqueous phase between these two states, it did not increase significantly, even if the quantity of

332 water injected at the soil surface (about 69 L) was localised in the investigated volume. Indeed,  
333 the volume of the soil aqueous phase was 51.9 L at 8.5 d and 123.7 L at 9.22 d.

334 The same observations were done for the 2<sup>nd</sup> experiment. Indeed, CO<sub>2</sub> mass decreased  
335 after the artificial rainfall event (6.17 d) by a factor of 2.1. The CO<sub>2</sub> amount in aqueous phase  
336 did not significantly vary. The mass balance also shows that the mass of CO<sub>2</sub> lost in the gas  
337 phase between 6.0 and 6.17 days is equivalent to the one lost at the top of the lysimeter. After  
338 day 6.34 of this 2<sup>nd</sup> experiment, a return at steady state conditions is observed (11 d) (Figure 7).  
339 Indeed, the water added begun to flow out of the investigated volume and the CO<sub>2</sub> mass in the  
340 gaseous phase begun to increase. A decrease, between 0.79 and 1.57 g of CO<sub>2</sub> in the aqueous  
341 phase is observed (Table 2).

### 342 3.5. Influence of natural rainfall events

343 The temporal evolution of precipitations and soil moisture content after the 2<sup>nd</sup> rainfall  
344 event are presented in Figure 9. The rainfall events modify directly soil moisture content even  
345 during a light and short-term rain. However, the depth of soil moisture modification varies  
346 according to the rainfall intensity and duration. For example, during the light and short-term  
347 rains between 20 and 22 d, a little increase of soil moisture could be only observed at 0.07 m  
348 depth whereas during the light and longer-term rainfall events (18 d - 19 d), the water contents  
349 were modified at 0.07 and 0.37 m depth (Figure 9-C and D). During the heavy natural rainfall  
350 events highlighted in blue (Figure 9-C), soil moisture increased at every depth.

351

352

353

354

355

356

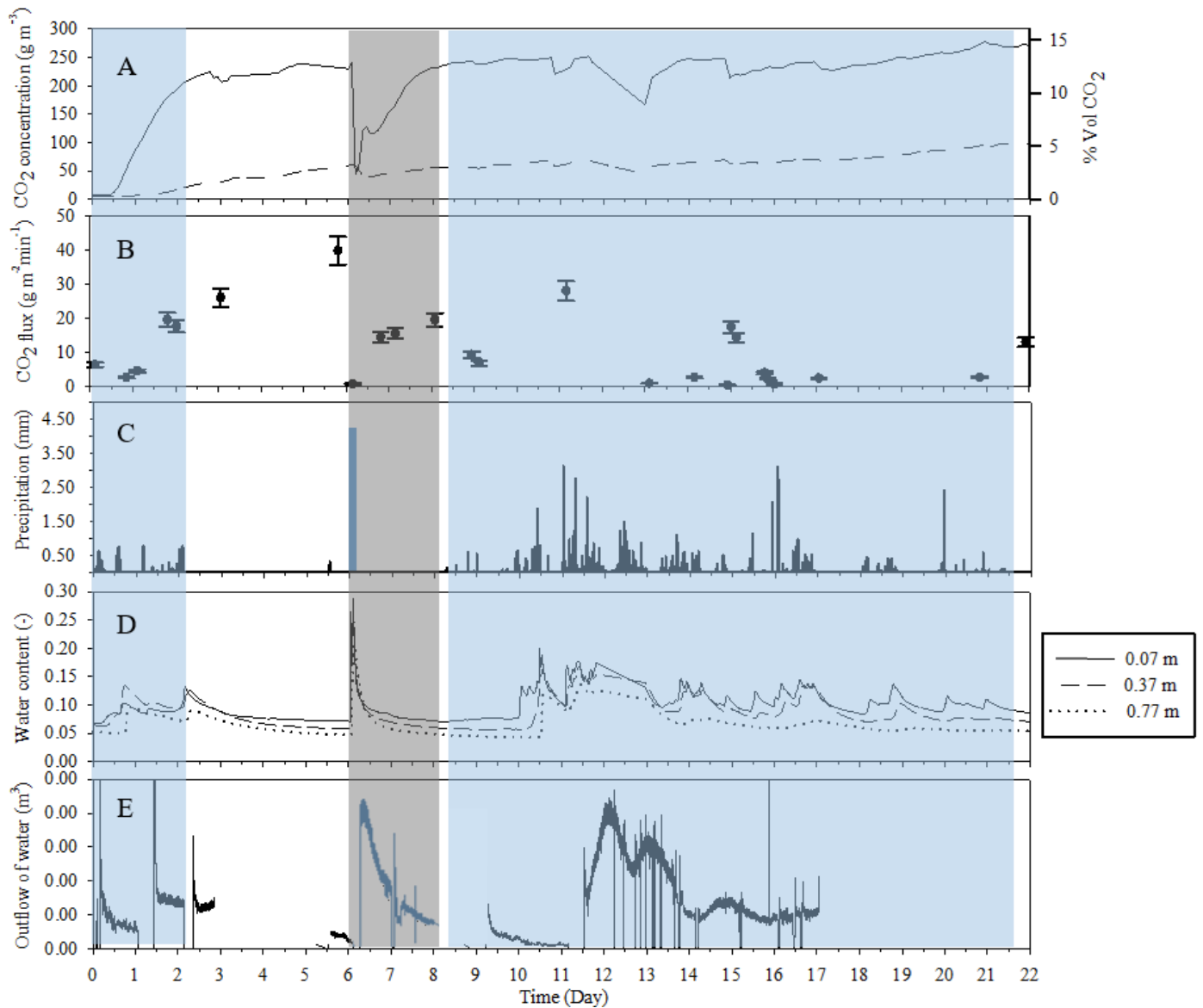


Figure 9. For the October experiment, times series of (A) CO<sub>2</sub> soil gas concentrations measured at 0.4 (solid line) and 0.8 m (short dash) depth, (B) CO<sub>2</sub> soil surface fluxes, in the centre of the lysimeter, (C) precipitation, the heavy rain are highlighted, (D) relative soil moisture at 0.07, 0.37 and 0.77 m depth and (E) outflow of water recorded during natural rainfall events from 8 d to 22 d of the October experiment. The data obtained after the artificial rainfall event are highlighted in grey.

357

358           The evolution of CO<sub>2</sub> soil gas concentrations and CO<sub>2</sub> fluxes at lysimeter surface during

359 natural rainfall events are also shown in Figure 9. The evolution of CO<sub>2</sub> fluxes showed a

360 relationship with the relative soil moisture (Figure 9-B, C and D) The CO<sub>2</sub> fluxes can be

361 analysed between day 13 and 17 where enough measurements could be done (Figure 9-B).

362 Between day 13 and 15, the effect of the heavy rainfall identified through the high water content

363 seem to lead to very low values of CO<sub>2</sub> fluxes (below 1 mg m<sup>-2</sup> min<sup>-1</sup>), despite the still high CO<sub>2</sub>  
 364 concentrations in the soil. These values are even lower than the one observed during or after  
 365 the artificial event. This may be linked to the higher water content than during the artificial  
 366 event period. During a short period, at day 15, some values of significant fluxes, close to the  
 367 one after the artificial rainfall event, are observed ( $\approx 17.5$  mg m<sup>-2</sup> min<sup>-1</sup>). They occur in a period  
 368 where the soil water content decreases and reaches values close to the one observed after the  
 369 rainfall event. However, when the water content increases again, the fluxes become negligible  
 370 again. Despite few values a similar behaviour could be observed at day 21 and 22 where a  
 371 decrease of water content seems to lead to high CO<sub>2</sub> fluxes values.

## 372 4. Discussion

### 373 4.1. Soil CO<sub>2</sub> diffusivities

374 During the artificial rainfall event, the increase of soil moisture content impacted CO<sub>2</sub>  
 375 soil gas fluxes. The Figure 10 shows the good accordance between CO<sub>2</sub> fluxes measurements  
 376 and CO<sub>2</sub> concentration gradients calculated between 0 and 0.4 m depth at the beginning of the  
 377 CO<sub>2</sub> injection until steady state.

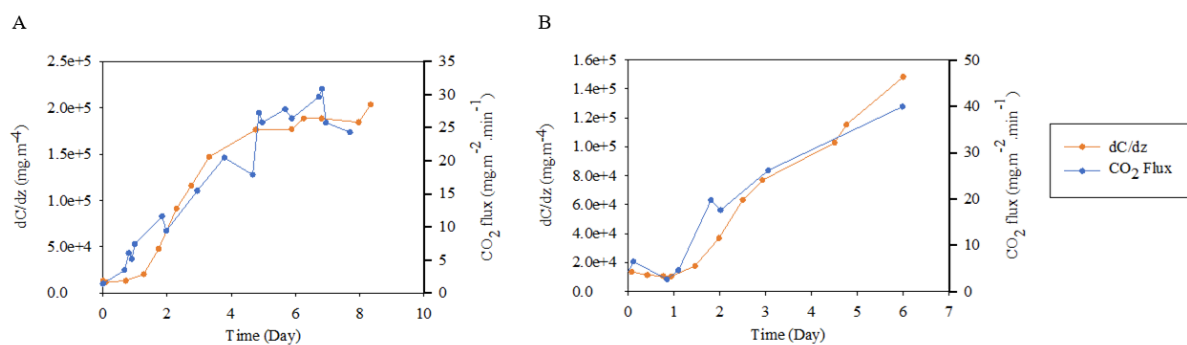


Figure 10. Relationship between CO<sub>2</sub> fluxes measurements and CO<sub>2</sub> concentration gradients (0 - 0.4 m depth) during February experiment (A) and October experiment (B).

378

379 According to first Fick law, the CO<sub>2</sub> flux ( $F_{CO_2}$ ) and CO<sub>2</sub> concentration are related  
 380 through the effective diffusion coefficient ( $D_e$ ):

381  $F = D_e \times \frac{dC}{dz}$  (6)

382 Even if atmospheric pressure varied during the experiments, Atteia and Höhener (2010)  
 383 showed that advective fluxes play a significant role only when the water saturation is very close  
 384 one, which never occur during the experiment.

385 Therefore, the experimental  $D_e$  can be calculated using eq. 6 and results from Figure 10. For  
 386 both experiment,  $D_e$  was calculated at steady state (8.5 and 6.0 d) and after the rainfall event  
 387 (9.22 and 6.17 d) on the first 40 centimetres (Table 3). The experimental  $D_e$  were compared to  
 388 the one predicted by classical empirical formulae in Table 3. Indeed,  $D_e$  can be estimated with  
 389 the molecular diffusivity of  $\text{CO}_2$  in air and an empirical tortuosity factors ( $\tau$ ) which was  
 390 determined in function of gas-phase ( $\Theta_g$ ) and total ( $\Theta$ ) porosity.  $\tau$  was estimated according to  
 391 the relationships of Moldrup (2000)  $\tau = \Theta_g^{2.5}/\Theta$ , Millington and Quirk (1961)  $\tau = \Theta_g^{10/3}/\Theta^2$ ,  
 392 Millington (1959)  $\tau = \Theta_g^{7/3}/\Theta^2$  and Penman (1940)  $\tau = 0.66 \times \Theta_g$ . These calculations were  
 393 based on the experimental measurements (Figure 3).

394 Table 3. Effect of soil air-filled porosity on the measured effective diffusion coefficient and  
 395 comparison with values calculated by empirical methods.

Experiment		1st		2nd	
		At steady state	After artificial rainfall event	At steady state	After artificial rainfall event
Soil moisture content (0 to 0.4 m depth) (-)		0.09	0.24	0.13	0.245
Experimental $D_e$ ( $\text{m}^2 \text{s}^{-1}$ )		$2.35 \times 10^{-6} \pm 2.4 \times 10^{-7}$	$9.48 \times 10^{-7} \pm 9.7 \times 10^{-8}$	$4.66 \times 10^{-6} \pm 4.8 \times 10^{-7}$	$9.30 \times 10^{-8} \pm 9.5 \times 10^{-9}$
Estimated $D_e^a$ ( $\text{m}^2 \text{s}^{-1}$ )	Moldrup et al. (2000)	$1.19 \times 10^{-6}$	$2.57 \times 10^{-7}$	$7.53 \times 10^{-7}$	$8.87 \times 10^{-8}$
	Millington and Quirk (1961)	$1.1 \times 10^{-6}$	$4.17 \times 10^{-8}$	$5.97 \times 10^{-7}$	$3.45 \times 10^{-8}$
	Millington (1959)	$4.57 \times 10^{-6}$	$4.63 \times 10^{-7}$	$2.99 \times 10^{-6}$	$4.05 \times 10^{-7}$
	Penman (1940)	$2.20 \times 10^{-6}$	$8.26 \times 10^{-7}$	$1.83 \times 10^{-6}$	$7.80 \times 10^{-7}$

396 <sup>a</sup> Free-air diffusion coefficient used for calculation were  $D_{\text{air}} \text{CO}_2 = 1.39 \times 10^{-5} \text{ m}^2 \text{ s}^{-1}$  (Pritchard and Currie, 1982)

397

398 As expected,  $D_e$  decreases with the increase of soil moisture content (Hers et al., 2000;  
 399 Jassal et al., 2005). According to the 1<sup>st</sup> experiment results, at steady state (8.5 and 6 d),  $D_e$  was

400 about  $2.35 \times 10^{-6} \text{ m}^2 \text{ s}^{-1}$  and decreased drastically after the artificial rainfall event (9.22 d) to  
401  $9.48 \times 10^{-7} \text{ m}^2 \text{ s}^{-1}$ . The same observation can be done for the 2<sup>nd</sup> experiment.

402 Overall, the comparisons between experimental and calculated  $D_e$  indicate that the  
403 Penman and Millington (1959) relationships provide correct estimates. Indeed, the  $D_e$  were  
404 similar or close by a factor of 0.55 to 2.55.

405 An exception was found for the estimated  $D_e$ , during the second experiment (after  
406 artificial rainfall event), where the estimated  $D_e$  calculated with the Moldrup relationship  
407 seemed approaching to experimental value with  $D_e$  of  $8.87 \times 10^{-8} \text{ m}^2 \text{ s}^{-1}$  and  $9.30 \times 10^{-8} \text{ m}^2 \text{ s}^{-1}$ ,  
408 respectively.

409 Hers et al. (2000) also observed a difference of the same order of magnitude between  
410 the measured and predicted values. They obtained a good comparison between the measured  
411 gas-phase tortuosity factor and the one predicted using the Millington and Quirk relationship  
412 with measured tortuosity factors about twice the predicted values.

413 These differences could be partly explained by the uncertainties in the experimental  
414 measures on the  $\text{CO}_2$  flux, soil moisture contents and soil  $\text{CO}_2$  concentrations.

#### 415 4.2. Influence of rainfall events

416 Few studies, to our knowledge, tried understanding the impacts of rainfall events on the  
417  $\text{CO}_2$  leakages to the environment and more particularly their influence on the  $\text{CO}_2$  diffusion  
418 along soil profile and  $\text{CO}_2$  fluxes (Oh et al., 2019; Seo et al., 2020). Understanding mechanisms  
419 is however crucial to advance modelling approaches to simulate  $\text{CO}_2$  flux surfaces under  
420 changing environmental conditions.

##### 421 4.2.1. Artificial rainfall event

422 After the artificial rainfall events, soil moisture content firstly increased while a  
423 significant decrease of soil  $\text{CO}_2$  concentrations and  $\text{CO}_2$  fluxes was observed. After this,  $\text{CO}_2$



424 concentrations and soil water contents reached back the steady state values at approximately 2  
425 days. The recovery process was longer for CO<sub>2</sub> fluxes. However, for both experiments, the  
426 return to the steady state of CO<sub>2</sub> fluxes was not observed. During the 1<sup>st</sup> experiment, it is  
427 possible that the measurement was stopped before the end of the recovery step. For the 2<sup>nd</sup>  
428 experiment, the heavy natural rainfall prevented the observation of the return to steady state.

429 A similar behaviour was observed by Lewicki et al. (2009) and Tommasone Pascale al.  
430 (2015). During a CO<sub>2</sub> release experiment, Lewicki et al. (2009) observed a decrease of CO<sub>2</sub>  
431 concentration which could have been partially due to changes in soil physical properties  
432 associated with significant rainfall events (10 – 20 mm). However, this effect of precipitations  
433 was not observed on the CO<sub>2</sub> fluxes. Tommasone Pascale al. (2015) studied the effect of  
434 rainstorm events on <sup>222</sup>Rn activity in soil, and observed an immediate drop in <sup>222</sup>Rn activities  
435 by several orders of magnitude after rainfall events. At the end of precipitation, soil <sup>222</sup>Rn  
436 activities did not appear to recover rapidly, at least for a time span of about a couple of days  
437 after storm ending. Tommasone Pascale et al (2015) shared the hypothesis given by Garcia-  
438 Vindas and Monnin (2005) stating that the immediate drop in <sup>222</sup>Rn activities following rainfall  
439 events are attributed to the dissolution of <sup>222</sup>Rn into the infiltrated water. This step consists in  
440 the “wash-out step” during which rainfall water infiltrates into the pore network and  
441 progressively washes out the radon, likely transferring to lower levels of the profile. Besides  
442 the different chemical behaviour of <sup>222</sup>Rn and CO<sub>2</sub> (e.g. production and decay), the present study  
443 seems to support this hypothesis. Indeed, a clear decrease of the total CO<sub>2</sub> mass was observed  
444 after the artificial rainfall event (Table 1).

445 In the mass balance calculations, the loss of CO<sub>2</sub> in the considered volume was like the  
446 loss measured at the soil surface. This implies that there is no entering flux of CO<sub>2</sub> from the  
447 source located below 80 cm while it is still providing a flux of CO<sub>2</sub>. One potential explanation,  
448 which is already cited by Viveiros et al. (2008), is that during a significant rainfall event the

449 soil gas is blocked below the infiltrated water. In that case, there could be a significant advective  
450 downward soil gas flux that would prevent the arrival of high CO<sub>2</sub> gas from the source.

451 Concerning the slow recovery stage of gas concentrations, there was no explication or  
452 hypothesis established in the literature at our knowledge. The results showed that the CO<sub>2</sub>  
453 profiles went overall back to steady state after 2.37 days from the beginning of rainfall event  
454 for the 1<sup>st</sup> experiment and 1.87 days for the 2<sup>nd</sup> experiment (Figure 7). However, observation  
455 data indicate that depending on depth CO<sub>2</sub> concentrations were not exactly back to steady state  
456 at the same time. For example, during the 1<sup>st</sup> experiment, CO<sub>2</sub> concentration at 0.8 m depth was  
457 back to steady state after about 2.46 and after 4.3 d at 0.4 m depth. The longer of recovery time  
458 lag at shallow depth may explain the slow recovery process of CO<sub>2</sub> flux. It would have been  
459 interesting to follow the temporal evolution of CO<sub>2</sub> concentrations at different depths between  
460 the surface and 0.4 m depth to confirm the time lag effect.

#### 461 4.2.2. Influence of natural rainfall events

462 During the 2<sup>nd</sup> experiment, different intensities of precipitation impacted CO<sub>2</sub> fluxes  
463 differently. The low-amplitude rainfall events and short-lived (estimated at less than 1-2 mm)  
464 cause a temporary mere wetting of the first centimetres of the ground surface which does not  
465 or barely affects soil CO<sub>2</sub> concentrations and flux. On the contrary, significant rainfall events  
466 (higher than 2 mm) appear to produce a clear decrease of CO<sub>2</sub> fluxes, owing by increase of soil  
467 moisture content in deeper. Tommasone Pascale et al (2015) also observed the modifications  
468 of <sup>222</sup>Rn activities deriving from significant rainfall depend on rainfall duration, persistency,  
469 and intensity.

## 470 5. Conclusion

471 The effect of rainfall events on soil gas flux was experimentally studied with lysimeter  
472 experiments. Rainfall and soil moisture have caused significant modifications in soil CO<sub>2</sub>

473 concentrations and flux during both experiments. During persistent and significant rainfall, the  
474 results clearly show a significant decrease of CO<sub>2</sub> flux to atmosphere induced by rainfall  
475 infiltration and consequential wash-out of the CO<sub>2</sub> present in the soil. After rainfall events, the  
476 recovery processes of soil CO<sub>2</sub> concentrations and fluxes were found to be very slow after the  
477 end of the artificial rainfall. Moreover, it can be expected that the temporal evolution of soil  
478 CO<sub>2</sub> concentrations is markedly dependent on the rainfall history of the site (total rainfall  
479 intensity, frequency and duration, intervals between rainfall events...) and the soil  
480 hydrodynamic properties. It should be noted that these experiments simulated conditions with  
481 high CO<sub>2</sub> concentrations like conditions encountered at CO<sub>2</sub> storage sites or petroleum-  
482 contaminated sites with high degradation rates. The conclusions can perhaps not be generalized  
483 to other sites with low CO<sub>2</sub> concentrations, e.g. in arid climates where water infiltration could  
484 stimulate respiration. In the present case, respiration in the vadose zone was assumed to be low  
485 and independent on moisture content.

486         Complementary studies are needed to understand and take into account all parameters  
487 that drive CO<sub>2</sub> diffusion along soil profile and CO<sub>2</sub> fluxes at the soil-atmosphere interface.  
488 Understanding these mechanisms is crucial in order to advance modelling approaches to predict  
489 CO<sub>2</sub> surfaces flux under changing environmental conditions.

490

#### 491 Acknowledgement

492 The authors would like to thank the partner companies of the INNOVASOL consortium  
493 which permitted to realize this research project.

494

495

- 497  
498 Atteia, O., Höhener, P., 2010. Semianalytical Model Predicting Transfer of Volatile Pollutants  
499 from Groundwater to the Soil Surface. *Environ. Sci. Technol.* 44, 6228–6232.  
500 <https://doi.org/10.1021/es903477f>
- 501 Beaubien, S.E., Jones, D.G., Gal, F., Barkwith, A.K.A.P., Braibant, G., Baubron, J.-C., Ciotoli,  
502 G., Graziani, S., Lister, T.R., Lombardi, S., Michel, K., Quattrocchi, F., Strutt, M.H.,  
503 2013. Monitoring of near-surface gas geochemistry at the Weyburn, Canada, CO<sub>2</sub>-EOR  
504 site, 2001–2011. *Int. J. Greenh. Gas Control*, The IEAGHG Weyburn-Midale CO<sub>2</sub>  
505 Monitoring and Storage Project 16, S236–S262.  
506 <https://doi.org/10.1016/j.ijggc.2013.01.013>
- 507 Bekele, D.N., Naidu, R., Chadalavada, S., 2014. Influence of spatial and temporal variability  
508 of subsurface soil moisture and temperature on vapour intrusion. *Atmos. Environ.* 88,  
509 14–22. <https://doi.org/10.1016/j.atmosenv.2014.01.053>
- 510 Bernardo, C., Vries, D.F. de, 2011. Permanent shallow subsoil CO<sub>2</sub> flux chambers for  
511 monitoring of onshore CO<sub>2</sub> geological storage sites. *Int. J. Greenh. Gas Control*, The  
512 5th Trondheim Conference on CO<sub>2</sub> Capture, Transport and Storage 5, 565–570.  
513 <https://doi.org/10.1016/j.ijggc.2010.05.011>
- 514 Bornemann, F., 1920. Kohlendensäure und Pflanzenwachstum. *Mitt. Dtsch. Landwirtsch.-Ges.*  
515 35:363.
- 516 Choi, J.-W., Smith, J.A., 2005. Geoenvironmental Factors Affecting Organic Vapor Advection  
517 and Diffusion Fluxes from the Unsaturated Zone to the Atmosphere under Natural  
518 Conditions. *Environ. Eng. Sci.* 22, 95–108. <https://doi.org/10.1089/ees.2005.22.95>
- 519 Conant, B.H., Gillham, R.W., Mendoza, C.A., 1996. Vapor Transport of Trichloroethylene in  
520 the Unsaturated Zone: Field and Numerical Modeling Investigations.  
521 <https://doi.org/10.1029/95WR02965>
- 522 Cotel, S., Schaefer, G., Sylvie, T., Marzougui-Jaafar, S., Gay, G., Razakarisoa, O., 2015.  
523 Evaluation of VOC fluxes at the soil-air interface using different flux chambers and a  
524 quasi-analytical approach. *Water. Air. Soil Pollut.* 226. [https://doi.org/10.1007/s11270-](https://doi.org/10.1007/s11270-015-2596-y)  
525 [015-2596-y](https://doi.org/10.1007/s11270-015-2596-y)
- 526 Elío, J., Nisi, B., Ortega, M.F., Mazadiego, L.F., Vaselli, O., Grandia, F., 2013. CO<sub>2</sub> soil flux  
527 baseline at the technological development plant for CO<sub>2</sub> injection at Hontomin (Burgos,  
528 Spain). *Int. J. Greenh. Gas Control* 18, 224–236.  
529 <https://doi.org/10.1016/j.ijggc.2013.07.013>
- 530 Elío, J., Ortega, M.F., Nisi, B., Mazadiego, L.F., Vaselli, O., Caballero, J., Chacón, E., 2016. A  
531 multi-statistical approach for estimating the total output of CO<sub>2</sub> from diffuse soil  
532 degassing by the accumulation chamber method. *Int. J. Greenh. Gas Control* 47, 351–  
533 363. <https://doi.org/10.1016/j.ijggc.2016.02.012>
- 534 Fa, K.-Y., Liu, J.-B., Zhang, Y.-Q., Wu, B., Qin, S.-G., Feng, W., Lai, Z.-R., 2015. CO<sub>2</sub>  
535 absorption of sandy soil induced by rainfall pulses in a desert ecosystem. *Hydrol.*  
536 *Process.* 29, 2043–2051. <https://doi.org/10.1002/hyp.10350>
- 537 Garcia-Vindas, J.R., Monnin, M.M., 2005. Radon concentration measurements in the presence  
538 of water and its consequences for Earth sciences studies. *Radiat. Meas.* 39, 319–322.  
539 <https://doi.org/10.1016/j.radmeas.2004.06.014>
- 540 Hers, I., Li, L., Hannam, S., 2004. Evaluation of soil gas sampling and analysis techniques at a  
541 former petrochemical plant site. *Environ. Technol.* 25, 847–860.  
542 <https://doi.org/10.1080/09593330.2004.9619377>

543 Hers, I., Zapf-Gilje, R., Li, L., Atwater, J., 2000. Measurement of in Situ Gas-Phase Diffusion  
544 Coefficients. *Environ. Technol.* 21, 631–640.  
545 <https://doi.org/10.1080/09593330.2000.9618948>

546 Jassal, R., Black, A., Novak, M., Morgenstern, K., Nestic, Z., Gaumont-Guay, D., 2005.  
547 Relationship between soil CO<sub>2</sub> concentrations and forest-floor CO<sub>2</sub> effluxes. *Agric.  
548 For. Meteorol.* 130, 176–192. <https://doi.org/10.1016/j.agrformet.2005.03.005>

549 Kim, J., Yu, S., Yun, S.-T., Kim, K.-H., Kim, J.-H., Shinn, Y.-J., Chae, G., 2019. CO<sub>2</sub> leakage  
550 detection in the near-surface above natural CO<sub>2</sub>-rich water aquifer using soil gas  
551 monitoring. *Int. J. Greenh. Gas Control* 88, 261–271.  
552 <https://doi.org/10.1016/j.ijggc.2019.06.015>

553 Klenbusch, M., 1986. Measurement of Gaseous Emission Rates From Land Surfaces Using an  
554 Emission Isolation Flux Chamber: User's Guide. US Environ. Prot. Agency Wash. DC  
555 EPA6008-86008.

556 Lelli, M., Raco, B., 2017. A reliable and effective methodology to monitor CO<sub>2</sub> flux from soil:  
557 The case of Lipari Island (Sicily, Italy). *Appl. Geochem.* 85, 73–85.  
558 <https://doi.org/10.1016/j.apgeochem.2017.08.004>

559 Lewicki, J.L., Hilley, G.E., Dobeck, L., Spangler, L., 2009. Dynamics of CO<sub>2</sub> fluxes and  
560 concentrations during a shallow subsurface CO<sub>2</sub> release. *Environ. Earth Sci.*

561 Ma, J., Zheng, X.-J., Li, Y., 2012. The response of CO<sub>2</sub> flux to rain pulses at a saline desert.  
562 *Hydrol. Process.* 26, 4029–4037. <https://doi.org/10.1002/hyp.9204>

563 Matthias, A.D., Blackmer, A.M., Bremner, J.M., 1980. A Simple Chamber Technique for Field  
564 Measurement of Emissions of Nitrous Oxide from Soils. *J. Environ. Qual.* 9, 251–256.  
565 <https://doi.org/10.2134/jeq1980.00472425000900020017x>

566 Millington, R.J., 1959. Gas Diffusion in Porous Media. *Science* 130, 100–102.  
567 <https://doi.org/10.1126/science.130.3367.100-a>

568 Millington, R.J., Quirk, J.P., 1961. Permeability of porous solids. *Trans. Faraday Soc.* 57, 1200–  
569 1207. <https://doi.org/10.1039/TF9615701200>

570 Moldrup, P., Olesen, T., Gamst, J., Schjønning, P., Yamaguchi, T., Rolston, D.E., 2000.  
571 Predicting the Gas Diffusion Coefficient in Repacked Soil Water-Induced Linear  
572 Reduction Model. *Soil Sci. Soc. Am. J.* 64, 1588–1594.  
573 <https://doi.org/10.2136/sssaj2000.6451588x>

574 Norman, J.M., Kucharik, C.J., Gower, S.T., Baldocchi, D.D., Crill, P.M., Rayment, M., Savage,  
575 K., Striegl, R.G., 1997. A comparison of six methods for measuring soil-surface carbon  
576 dioxide fluxes. *J. Geophys. Res. Atmospheres* 102, 28771–28777.  
577 <https://doi.org/10.1029/97JD01440>

578 Oh, Y.Y., Yun, S.T., Yu, S., Kim, H.J., Jun, S.C., 2019. A novel wavelet-based approach to  
579 characterize dynamic environmental factors controlling short-term soil surface CO<sub>2</sub>  
580 flux: Application to a controlled CO<sub>2</sub> release test site (EIT) in South Korea. *Geoderma*  
581 337, 76–90. <https://doi.org/10.1016/j.geoderma.2018.09.017>

582 Palaia, T., Jimmo, A., Mahler, N., Molinari, C., Clements, L., 2018. Technical measurement  
583 guidance for LNAPL natural source zone depletion. CRC CARE Tech. Rep. No 44 254.  
584 <https://doi.org/10.1089/ees.2005.22.95>

585 Penman, H.L., 1940. Gas and vapour movements in the soil: I. The diffusion of vapours through  
586 porous solids. *J. Agric. Sci.* 30, 437–462. <https://doi.org/10.1017/S0021859600048164>

587 Petersen, L.W. (Danish I. of P. and S.S., El-Farhan, Y.H., Moldrup, P., Rolston, D.E.,  
588 Yamaguchi, T., 1996. Transient diffusion, adsorption, and emission of volatile organic  
589 vapors in soils with fluctuating low water contents. *J. Environ. Qual. USA.*

590 Reinhart, D.R., Cooper, D.C., Walker, B.L., 1992. Flux Chamber Design and Operation for the  
591 Measurement of Municipal Solid Waste Landfill Gas Emission Rates. *J. Air Waste  
592 Manag. Assoc.* 42, 1067–1070. <https://doi.org/10.1080/10473289.1992.10467053>

593 Risk, D.A., Kellman, L.M., Beltrami, H., 2002. Soil CO<sub>2</sub> production and surface flux at four  
594 climate observatories in eastern Canada. <https://doi.org/10.1029/2001GB001831>

595 Rochette, P., Hutchinson, G., 2005. Measurement of Soil Respiration in situ: Chamber  
596 Techniques. Publ. USDA-ARS UNL Fac.

597 Rodier, J., 1976. L'analyse de l'eau. Eaux naturelles, eaux résiduaires, eaux de mer., Dunod  
598 Tech, Bordas, Paris. ed.

599 Sander, S.P., Friedl, R.R., Barker, J.R., Abbatt, J.P.D., Burkholder, J.B., Friedl, R.R., Golden,  
600 D.M., Huie, R.E., Kolb, C.E., Kurylo, M.J., Moortgat, G.K., Orkin, V.L., Wine, P.H.,  
601 2011. Chemical Kinetics and Photochemical Data for Use in Atmospheric Studies  
602 Evaluation No. 17. JPL Publ. 10–6, Jet Propulsion Laboratory, Pasadena, 684.

603 Schroder, I.F., Zhang, H., Zhang, C., Feitz, A.J., 2016. The role of soil flux and soil gas  
604 monitoring in the characterisation of a CO<sub>2</sub> surface leak: A case study in Qinghai,  
605 China. *Int. J. Greenh. Gas Control* 54, 84–95.  
606 <https://doi.org/10.1016/j.ijggc.2016.07.030>

607 Seo, D.H., Han, W.S., Park, E., Jeong, J., Oh, Y.-Y., Kim, H.-J., Yoo, G., Jun, S.-C., Yun, S.-  
608 T., 2020. Analyses and numerical evaluation of integrated time-series monitoring  
609 datasets including CO<sub>2</sub> concentration and fluxes at controlled CO<sub>2</sub> release site in South  
610 Korea. *J. Hydrol.* 590, 125213. <https://doi.org/10.1016/j.jhydrol.2020.125213>

611 Shao, H., Ussiri, D.A.N., Patterson, C.G., Locke, R.A., II, Wang, H., Taylor, A.H., Cohen, H.F.,  
612 2019. Soil gas monitoring at the Illinois Basin – Decatur Project carbon sequestration  
613 site. *Int. J. Greenh. Gas Control* 86, 112–124.  
614 <https://doi.org/10.1016/j.ijggc.2019.04.012>

615 Shen, R., Pennell, K.G., Suuberg, E.M., 2013. Influence of Soil Moisture on Soil Gas Vapor  
616 Concentration for Vapor Intrusion. *Environ. Eng. Sci.* 30, 628–637.  
617 <https://doi.org/10.1089/ees.2013.0133>

618 Shen, R., Pennell, K.G., Suuberg, E.M., 2012. A numerical investigation of vapor intrusion--  
619 the dynamic response of contaminant vapors to rainfall events. *Sci. Total Environ.* 437,  
620 110–120. <https://doi.org/10.1016/j.scitotenv.2012.07.054>

621 Smith, J.A., Tisdale, A.K., Cho, H.J., 1996. Quantification of Natural Vapor Fluxes of  
622 Trichloroethene in the Unsaturated Zone at Picatinny Arsenal, New Jersey. *Environ.*  
623 *Sci. Technol.* 30, 2243–2250. <https://doi.org/10.1021/es950610c>

624 Tillman, F.D., Smith, J.A., 2004. Design and laboratory testing of a chamber device to measure  
625 total flux of volatile organic compounds from the unsaturated zone under natural  
626 conditions. *J. Contam. Hydrol.* 75, 71–90.  
627 <https://doi.org/10.1016/j.jconhyd.2004.04.005>

628 Tommasone Pascale, F., Carbone, P., De Francesco, S., Cuoco, E., Tedesco, D., 2015.  
629 Rainstorm-induced soil <sup>222</sup>Rn concentration spikes observed in Southern Italy.  
630 *Environ. Earth Sci.* 73, 8177–8187. <https://doi.org/10.1007/s12665-014-3976-0>

631 Viveiros, F., Ferreira, T., Cabral Vieira, J., Silva, C., Gaspar, J.L., 2008. Environmental  
632 influences on soil CO<sub>2</sub> degassing at Furnas and Fogo volcanoes (São Miguel Island,  
633 Azores archipelago). *J. Volcanol. Geotherm. Res., Volcanic Flows and Falls* 177, 883–  
634 893. <https://doi.org/10.1016/j.jvolgeores.2008.07.005>

635 Werner, D., Grathwohl, P., Höhener, P., 2004. Review of Field Methods for the Determination  
636 of the Tortuosity and Effective Gas-Phase Diffusivity in the Vadose Zone. *Vadose Zone*  
637 *J.* 3, 1240–1248. <https://doi.org/10.2136/vzj2004.1240>

638 Wilke, B.-M., 2005. Determination of Chemical and Physical Soil Properties, in: Margesin, R.,  
639 Schinner, F. (Eds.), *Monitoring and Assessing Soil Bioremediation, Soil Biology.*  
640 Springer, Berlin, Heidelberg, pp. 47–95. [https://doi.org/10.1007/3-540-28904-6\\_2](https://doi.org/10.1007/3-540-28904-6_2)

641 Yang, L., Chen, Z., Zhang, X., Liu, Y., Xie, Y., 2015. Comparison study of landfill gas  
642 emissions from subtropical landfill with various phases: A case study in Wuhan, China.

643 J. Air Waste Manag. Assoc. 65, 980–986.  
644 <https://doi.org/10.1080/10962247.2015.1051605>  
645